Journal of Materials Chemistry A

ROYAL SOCIETY OF CHEMISTRY

PAPER

View Article Online
View Journal | View Issue

Cite this: J. Mater. Chem. A, 2024, 12, 3589

Multifunctional conductive hydrogels for wearable sensors and supercapacitors†

Quancai Li, Bin Tian,* Guilin Tang, Haoye Zhan, Jing Liang,* Panwang Guo, Qun Liu and Wei Wu *

Conductive hydrogels have attracted extensive attention in the field of flexible electronics due to their excellent biocompatibility, suitable Young's modulus, and outstanding electrical conductivity. However, the inherent water-rich feature and insufficient interfacial adhesion of hydrogels hinder the stability and reliability of hydrogel-based devices for applications in complex environments. Herein, we design a novel polyacrylamide/polydopamine hydrogel using deep eutectic solvent (DES) and alkaline solution as the polymerization medium, and the as-obtained hydrogel has both self-adhesive (20.20 kPa for tissue) and anti-freezing properties (−20 °C). The combination of DES and alkaline solution replaces pure DES, which provides the conditions for oxidative polymerization of dopamine to ensure the adhesion performance of the hydrogel and also makes the hydrogel retain the conductivity and low melting point characteristics of DES. Furthermore, biocompatible carboxylated cellulose nanofibers (CCNFs) are embedded into the hydrogel to further enhance the mechanical properties by about 3 times through non-covalent interactions, physical entanglement and friction between CCNFs and the polymer. Remarkably, the hydrogel can be adhered to the skin as a bioelectrode for electrocardiography and can be used as a strain sensor to monitor human movements even after storing for 15 days at −20 °C. Meanwhile, the electrochemical characterization of supercapacitors using this hydrogel as an electrolyte shows great application potential.

Received 6th November 2023
Accepted 3rd January 2024

DOI: 10.1039/d3ta06771h

rsc.li/materials-a

1. Introduction

Flexible electronic devices have developed rapidly in recent years, and their simple structure and convenient production process make them attract a lot of attention in the fields of motion signal monitoring, human–machine interface, and energy storage.[1–5] Traditional devices consist of a conducting layer and substrate, which are prone to separate due to mechanical matching issues.[6,7] Moreover, substrates such as polydimethylsiloxane (PDMS), Ecoflex, and other elastomers have high Young's modulus and limited deformation, which affect the practical application of the device.[8–11] Hydrogels are a kind of material with a large amount of water and a three-dimensional network structure with tissue-like Young's modulus and integrated structures.[12–14] In addition, hydrogels have become the most ideal materials for flexible electronics in the past decade due to their excellent biocompatibility and tunable conductive and mechanical properties.

However, the water in hydrogels is poorly tolerant to the environment, which greatly limits the application of hydrogels. Even when hydrogels are placed in a suitable environment, they may still become stiff and lose their performance after a period of time as the water evaporates. Furthermore, it is also necessary to endow hydrogels with the ability to work at sub-zero temperatures, which can prevent the water from freezing and expand the application scenarios.[15] To date, various strategies have been developed to improve the anti-freezing and moisturizing properties of hydrogels, including the addition of hygroscopic inorganic salts, organic solutions, ionic liquids, or the establishment of an isolation layer.[16–19] However, the aforementioned methods cannot meet the requirements of biocompatibility and cost-effectiveness, which limits the applications of hydrogel-based devices. Deep eutectic solvents (DESs) are a new class of green solvents, composed of a variety of components that can associate with each other through hydrogen bond interactions and have attracted a lot of attention recently due to their conductivity, low melting point, and low vapor pressure.[20] DESs exhibit similar properties to ionic liquids, while the low cost and non-toxic properties of DESs make them more potential and exploratory than the latter.[21] At the same time, these properties of DESs all meet the requirements of a new-generation of healthcare for sensing biological systems without eliciting undesirable responses, which promotes the development of DES-based hydrogels in flexible electronics.[22]

Laboratory of Printable Functional Materials and Printed Electronics, School of Physics and Technology, Wuhan University, Wuhan 430072, P. R. China. E-mail: bin.tian@whu.edu.cn; jingliang@whu.edu.cn; weiwu@whu.edu.cn; Fax: +86-27-68778433; Tel: +86-27-68778491

† Electronic supplementary information (ESI) available. See DOI: https://doi.org/10.1039/d3ta06771h

For flexible devices, most hydrogels require additional fixation devices before application, including tapes and bandages, which may have excessive adhesion to increase the difficulty of peeling and are uncomfortable for the wearer.[23] Moreover, the excellent self-adhesive properties can enhance the accuracy of electrical signals during physical deformation by forming a conformal contact to adapt to the complex surface of adherends.[24] To maximize the performance and ease of use of hydrogel-based devices, it is urgent to endow hydrogels with self-adhesive properties. To address this issue, mussel-inspired adhesive mechanisms have been extensively studied and polydopamine (PDA) based hydrogels have achieved self-adhesive properties due to carrying a large number of catechol groups with similar structures to mussels.[25–27] PDA can be obtained by oxidative polymerization of dopamine (DA) under alkaline conditions, and the catechol groups on PDA can establish interactions with organic or inorganic substrates to achieve robust adhesion.[28–30] This facile polymerization method provides convenience for the design of self-adhesive hydrogels. And the early research edified us to combine the mussel-inspired DA with the stunning characteristics of DESs to meet the demands of hydrogels for adhesion and extreme temperature for flexible electronics applications.

Herein, we designed carboxylated cellulose nanofibers (CCNFs) enhanced polyacrylamide (PAM)/PDA conductive hydrogels based on DES (HDES/CCNF) with good stretchability, and admirable self-adhesive, anti-freezing, and moisturizing properties (Fig. 1). Instead of pure DES, the mixed solution combined a DES and alkali solution as the medium for polymerization is the essential factor to design the HDES/CCNF hydrogel system. Notably, the mixed solution retaining the characteristics of DES including good ionic conductivity, low vapor pressure, and low melting point enables HDES/CCNF hydrogels with excellent conductivity (0.99 mS cm^{-1}), anti-freezing (−20 °C), and moisturizing properties. The presence of alkali solution can provide a reaction environment for the oxidative polymerization of DA to PDA, ensuring the self-adhesion of HDES/CCNF hydrogels. Additionally, the mixed solution can effectively increase the solubility of acrylamide (AM) to facilitate the construction of the hydrogel networks. Furthermore, owing to their nano-reinforcement effect, the addition of CCNFs greatly improved the mechanical properties of the hydrogel without affecting the conductivity, which is about 3 times that of the PAM/PDA conductive hydrogels based on DES (HDES). HDES/CCNF can not only be attached to the skin as a bioelectrode for electrocardiogram (ECG) recording, but can also be assembled into resistive stretchable strain sensors and capacitive pressure sensors for human motion detection. HDES/CCNF-based strain sensors exhibit a wide workable strain range, high linearity, and good dynamic stability. Meanwhile, HDES/CCNF can also be used as a solid electrolyte in supercapacitors for energy storage.

2. Experimental section

2.1 Preparation of DES_{EG}-based conductive hydrogels with CCNFs ($HDES_{EG}/CCNF_{n\%}$)

DES_{EG} and NaOH solution (pH = 11) were uniformly mixed at a volume ratio of 1 : 1 to obtain a mixed solution. Then carboxylated cellulose nanofibers (CCNFs) were added to the mixed solution for ultrasonication and vigorous stirring to disperse evenly. Dopamine (DA) was then added to the mixed solution and stirred thoroughly for 30 min to generate PDA. Acrylamide (AM), ammonium persulfate, and *N*,*N*-methylenebisacrylamide were further added to the mixed solution and stirred for 10 min, and then transferred to a mold (55 mm × 15 mm × 3 mm) and UV irradiated (365 nm, 7 W) for 30 min to obtain $HDES_{EG}/CCNF_{n\%}$ (n = 1, 2, 3, 4, and n represents the mass percentage of CCNFs to AM). The detailed ingredients of $HDES_{EG}/CCNF_n$ are shown in Table S3.†

2.2 Characterization and measurements

Hydrogels were lyophilized after being replaced with deionized water three times (one replacement every 12 hours), and the morphology of hydrogels was characterized with a cold field emission scanning electron microscope (SEM, Hitachi S-4800). Differential scanning calorimetry analysis (DSC) and thermogravimetric analysis (TGA) were performed on the hydrogel under a nitrogen atmosphere (Mettler-Toledo DSC3/TGA2). The temperature range and heating rate of DSC were −60–20 °C and 10 °C min^{-1}, and the mass of hydrogel was 10 mg. The temperature range and heating rate of TGA were 25–200 °C and 10 °C min^{-1}, and the mass of hydrogel was 10 mg. The ^{1}H-NMR spectra were recorded in dimethyl sulfoxide with a Bruker AVANCE NEO 600 spectrometer (600 MHz). A Keithley-2400 digital multimeter was used to record real-time resistance changes, and a DY-IS stepper motor controller cooperating with an electric linear table was used for strain control. Mechanical and adhesive properties were tested with an electric tensile testing machine (ZhiQu precision instruments, ZQ-990LA-5). A TH2832 LCR meter (Tonghui) was used to record real-time capacitance changes. A GW Instek GPP-4323 provided a power supply during the hydrogel energization test. Electrochemical testing including cyclic voltammetry (CV), galvanostatic charge/discharge (GCD), and electrochemical impedance spectroscopy (EIS) was performed with an electrochemical workstation (CH Instruments, CHI 760E) and capacitance retention was tested with a LAND CT3002A.

3. Results and discussion

3.1 Basic properties of the HDES hydrogel

Four DESs are prepared separately using polyols diethylene glycol, glycerol, ethylene glycol, and xylitol (DG, Gly, EG, and Xy) as hydrogen bond donors and choline chloride (ChCl) as the hydrogen bond acceptor. The chemical structures and photographs of DESs are shown in Fig. 2a and S1.† The conductive hydrogels prepared based on the four DESs are labeled $HDES_{DG}$, $HDES_{Gly}$, $HDES_{EG}$, and $HDES_{Xy}$, respectively. All four conductive hydrogels appear brown, which is the intrinsic color of PDA (Fig. S1†). The mechanical properties of HDESs are shown in Fig. 2a. The $HDES_{Xy}$ hydrogel exhibits the biggest tensile stress of 55.95 kPa and an elongation at break of 672.8%, which may cause the high viscosity of DES_{Xy} that can be more firmly integrated into the gel network.[20,31] $HDES_{DG}$, $HDES_{EG}$, and $HDES_{Gly}$

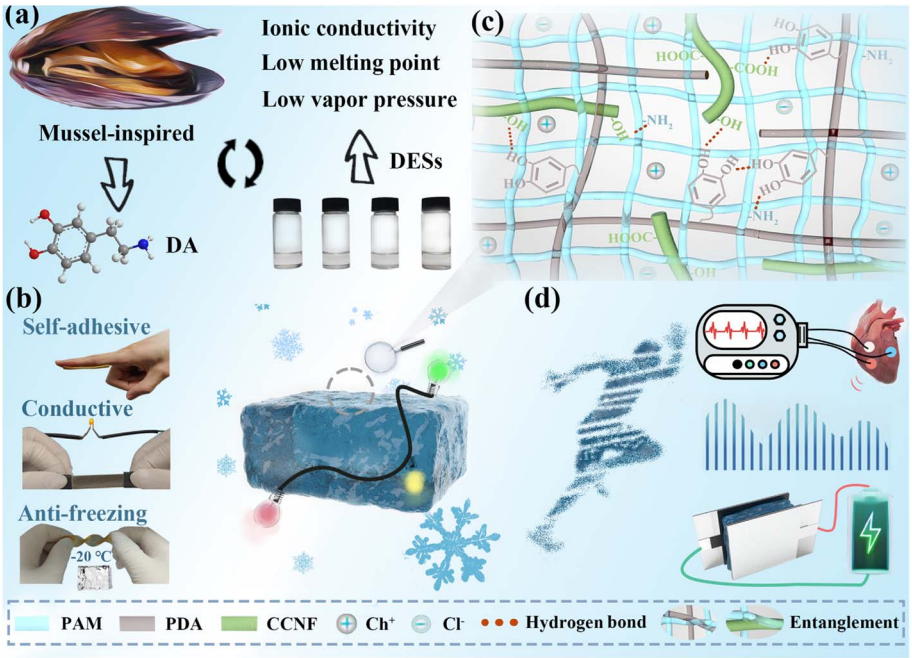

Fig. 1 Overview of the design strategy, performance and applications of DES/CCNF hydrogels. (a) The design strategy of self-adhesive, anti-freezing conductive hydrogels. (b) Schematic and performance demonstration of DES/CCNF hydrogels. (c) The internal network structure of DES/CCNF hydrogels and the interaction between components. (d) Schematic diagram of the applications of hydrogels in ECG testing, human motion monitoring, and supercapacitors.

hydrogels almost present similar tensile stress of about 20 kPa. Conductivity is another key parameter of conducting hydrogels. As shown illustrated in Fig. 2c and S2,† the ionic conductivity of $HDES_{DG}$, $HDES_{Gly}$, $HDES_{EG}$, and $HDES_{Xy}$ hydrogels calculated by electrochemical impedance spectroscopy (EIS) is 0.35 mS cm^{-1}, 0.30 mS cm^{-1}, 0.98 mS cm^{-1}, and 0.16 mS cm^{-1}, respectively. The $HDES_{EG}$ hydrogel with a good balance of mechanical and electrical properties is applied for further exploration.

The effect of the volume ratio of DES_{EG} and alkali solution (pH = 11) on the mechanical, electrical, and moisturizing properties of $HDES_{EG}$ hydrogels is further studied. $HDES_{EG}$ hydrogels based on the volume ratios of DES_{EG} and NaOH solution of 1 : 9, 3 : 7, 5 : 5, 7 : 3, and 9 : 1 are marked as $HDES_{EG1}$, $HDES_{EG3}$, $HDES_{EG5}$, $HDES_{EG7}$, and $HDES_{EG9}$, respectively. With the increase of DES_{EG} content, the tensile strength of $HDES_{EG}$ decreases and the elongation increases (Fig. 2d). The $HDES_{EG1}$ hydrogel achieves the highest tensile strength of 774.58 kPa and an elongation at break of 384.09%, while $HDES_{EG7}$ presents only 5.83 kPa and 925.95% correspondingly. $HDES_{EG9}$ exhibits a low degree of gelation due to insufficient dissolution of AM monomer, which is not discussed further here (Fig. S3†). Under an external electric field, Ch^+ ions and Cl^- ions migrate directionally to the cathode and anode, respectively, thereby forming a conductive path.[32,33] With the increase of DES_{EG} volume, the conductive properties of $HDES_{EG}$ hydrogels increase simultaneously as shown in Fig. 2e. The ionic conductivity of $HDES_{EG3}$, $HDES_{EG5}$, and $HDES_{EG7}$ hydrogels is 0.22 mS cm^{-1}, 0.98 mS cm^{-1}, and 1.11 mS cm^{-1}, while the $HDES_{EG1}$ hydrogel does not conduct electricity. The reasons for the above phenomena are explained as follows. First of all, samples are tested after one day of placement, and hydrogels with higher water content become more brittle with the evaporation of water, whereas hydrogels with high DES_{EG} content maintain softer properties due to the low vapor pressure of DES_{EG}. Additionally, excessive content of DES_{EG} affects the dissolution of AM and thus retards the polymerization of polymers resulting in a reduction in the mechanical strength of $HDES_{EG}$ hydrogels. For conductivity, the larger the proportion of DES_{EG}, the more Ch^+ ions and Cl^- ions are introduced into the $HDES_{EG}$ hydrogel and the sparse the polymer network, resulting in higher conductivity. At the same time, excessive water reduces the self-association between DES components and destroys the structure of DES.[34,35] Furthermore, the moisturizing performance of $HDES_{EG}$ hydrogels is heavily dependent on the proportion of DES_{EG} in Fig. 2f. After one day of placement, the weight ratios of $HDES_{EG1}$, $HDES_{EG3}$, $HDES_{EG5}$, $HDES_{EG7}$ hydrogels are 44.91%, 61.99%, 84.12%, and 98.42%, respectively. And the weight ratios after 7 days are 41.88%, 57.66%, 77.40%, and 92.97%, respectively. The thermogravimetric curves also prove that the weight loss of the hydrogel is less with the increase of DES content, indicating the better moisturizing properties of the hydrogel in Fig. S4.† The moisturizing performance of $HDES_{EG}$ hydrogels is attributed to the low vapor pressure of DES_{EG} and the ability to absorb moisture from the environment due to the strong interaction of DES_{EG} with water molecules.[35,36] The adhesion strength of hydrogels with different DES contents increases first and then decreases (Fig. S5†). When the DES content is small, the evaporation of water causes the hydrogel to become drier and the adhesion

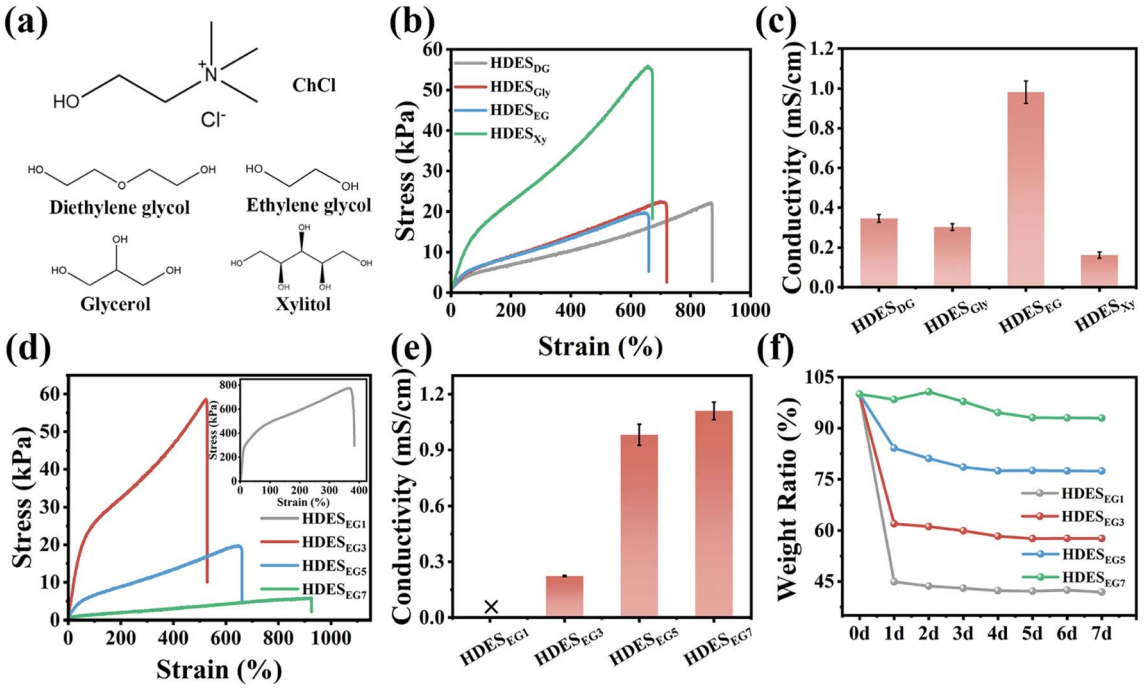

Fig. 2 (a) Chemical structure of the hydrogen bond acceptor (ChCl) and hydrogen bond donors (DG, EG, Gly, and Xy). (b) Stress–strain curves of the four hydrogels containing different DESs. (c) The conductivity of the four hydrogels containing different DESs. (d) Stress–strain curves of the four hydrogels with different ratios of DES_{EG}. (e) The conductivity of the four hydrogels with different ratios of DES_{EG}. (f) Changes in the weight ratios of the four hydrogels with different ratios of DES_{EG} over a week at room temperature.

strength decreases. $HDES_{EG3}$ exhibits the greatest adhesion strength, which is attributed to its certain wettability and the presence of catechol groups. The substantial reduction in the adhesion strength of $HDES_{EG7}$ is attributed to its low cohesion. Considering the basic properties of hydrogels comprehensively, the $HDES_{EG5}$ hydrogel is selected as the object of subsequent discussion.

3.2 Mechanical and conductive properties of the DES_{EG}/CCNF hydrogel

Although the $HDES_{EG5}$ hydrogel possesses excellent conductivity and moisturizing performance, the limited mechanical properties restrict the application of the hydrogel in the field of flexible electronics. To improve the ability to resist external deformation and obtain suitable Young's modulus, nanofillers have been widely used in hydrogel matrices according to the nano-enhancement effect.[37] Here, CCNFs are selected as the toughening agent to further improve the mechanical performance of $HDES_{EG}$ because of their excellent biocompatibility and water dispersibility.[38] $HDES_{EG5}$/CCNF hydrogels with the addition of CCNFs in amounts of 1%, 2%, 3%, and 4% are labeled $HDES_{EG}/CCNF_{1\%}$, $HDES_{EG}/CCNF_{2\%}$, $HDES_{EG}/CCNF_{3\%}$, and $HDES_{EG}/CCNF_{4\%}$, respectively. As shown in Fig. 3a, as the concentration of CCNFs increased from 1% to 4%, the fracture strength of the four $HDES_{EG}$/CCNF hydrogels is 26.44, 34.90, 58.80, and 76.22 kPa, respectively. And the maximum strain of $HDES_{EG}$/CCNF hydrogels can reach 639.14%, 492.81%, 416.68%, and 343.34% respectively. The mechanical strength is significantly improved compared to $HDES_{EG}$ due to the presence of CCNFs. It is worth noting that the increased concentration of CCNFs causes increased fracture stress and decreased maximum strain (Fig. 3b). Furthermore, the toughness and Young's modulus increase with the increase of CCNFs. As shown in Fig. 3c, when the content of CCNFs is 1% and 2%, the toughness and modulus of hydrogels are similar (difference of 3.5 kPa). The $HDES_{EG}/CCNF_{3\%}$ hydrogel possesses a toughness of 123.25 kJ m^{-3} and Young's modulus of 17.26 kPa. The $HDES_{EG}/CCNF_{4\%}$ hydrogel exhibits the maximum toughness and Young's modulus, which are 137.44 kJ m^{-3} and 27.11 kPa. These results are attributed to the presence of CCNFs in the hydrogel network. Besides the covalent cross-linked network of PAM in pure $HDES_{EG}$, the catechol groups on PDA chains can form interactions with amino groups of the gel skeleton.[39–41] As shown in Fig. S6,† the active hydrogen of DA shifts from 7.98 ppm to 7.86 ppm, and the two phenolic hydroxyl peaks (8.90 ppm and 8.84 ppm) turned into a sharp peak of 8.83 ppm.[40] These results indicate that there are interactions between AM and DA. Moreover, the interactions among PDA chains can provide effective energy dissipation, including hydrogen bonds and π–π stacking.[29] Microfibril structures in Fig. S7a and b† may be caused by these interactions. After adding CCNFs, there are more interactions in $HDES_{EG}$/CCNF hydrogels to enhance the mechanical properties (Fig. 1c). On the one hand, the surface of CCNFs possesses plenty of carboxyl groups and hydroxyl groups, which probably form hydrogen bonds with catechol groups of PDA and amino groups of PAM helping to dissipate energy when $HDES_{EG}$/CCNF hydrogels are

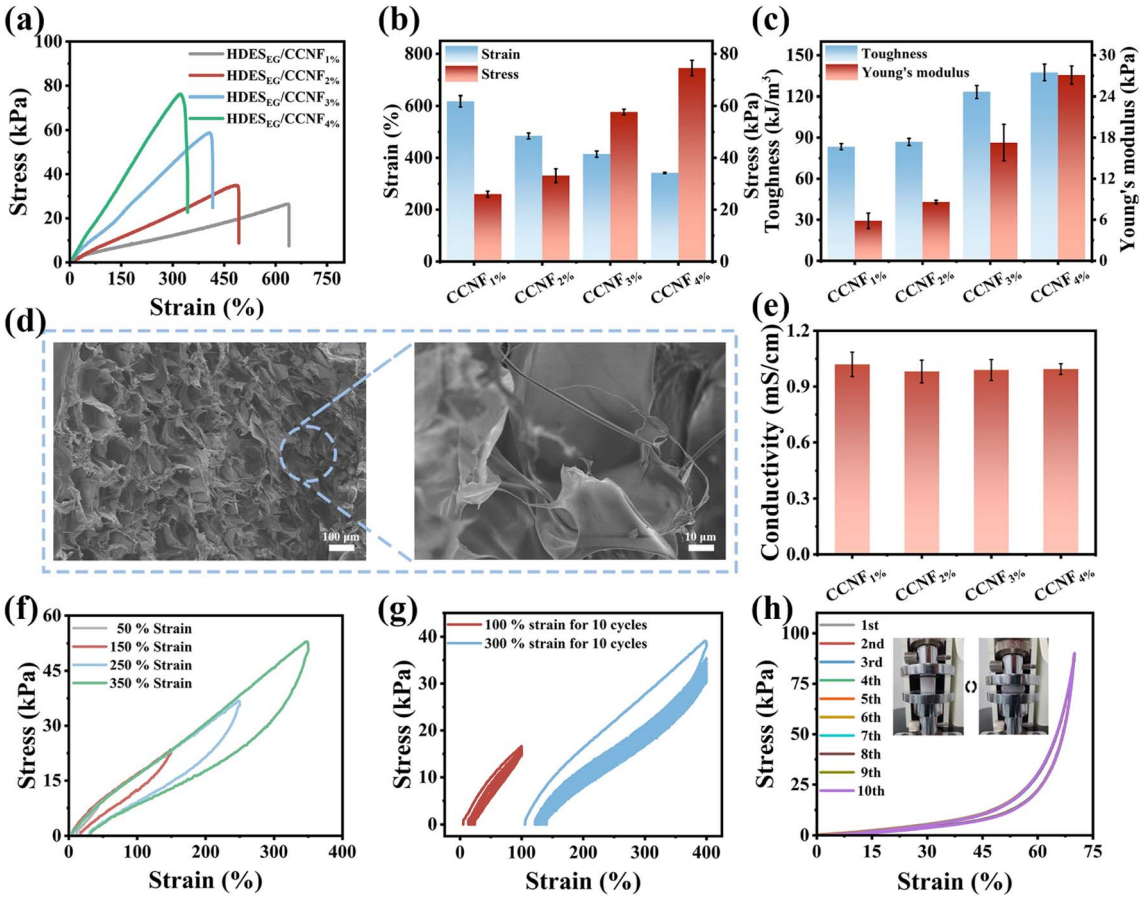

Fig. 3 (a) Stress–strain curves of the four HDES$_{EG}$/CCNF$_{n\%}$ hydrogels (n = 1, 2, 3, 4). (b) Strain and stress of HDES$_{EG}$/CCNF$_{n\%}$ (n = 1, 2, 3, 4). (c) Toughness and Young's modulus of HDES$_{EG}$/CCNF$_{n\%}$ (n = 1, 2, 3, 4). (d) SEM image of HDES$_{EG}$/CCNF$_{3\%}$ under different magnifications. (e) Conductivity of HDES$_{EG}$/CCNF$_{n\%}$ hydrogels (n = 1, 2, 3, 4). (f) Single loading-unloading cycle curves of HDES$_{EG}$/CCNF$_{3\%}$ hydrogels under different strains (50%, 150%, 250%, and 350%). (g) 10 cycles of loading-unloading curves of HDES$_{EG}$/CCNF$_{3\%}$ hydrogels without time interval at the strains of 100% and 300%. (h) Schematic diagram and compressive strength of 10 cycles of compression recovery of HDES$_{EG}$/CCNF$_{3\%}$ hydrogels at a strain of 70%.

stretched.[39,41–43] On the other hand, CCNFs can well embed into the network of HDES$_{EG}$/CCNF hydrogels and are entangled with the polymer chains to enhance the internal friction when external force occurs to improve the mechanical properties. The fibers in Fig. 3d may be CCNFs embedded in the hydrogel. All in all, the mechanical strength of hydrogels added with CCNFs is significantly improved compared with the HDES$_{EG}$ hydrogel attributed to the synergistic result of effective nano-reinforcement and physical interactions.

The addition of CCNFs does not cause a significant effect on the conductivity of the HDES$_{EG}$/CCNF hydrogels (Fig. 3e and S8†). It may be that the limited transport capacity of restricted cellulose content to bulky choline cations and the greater viscosity of the polymerization medium compared to water hinder ion transport.[44,45] The conductivity of HDES$_{EG}$/CCNF$_{1\%}$, HDES$_{EG}$/CCNF$_{2\%}$, HDES$_{EG}$/CCNF$_{3\%}$, and HDES$_{EG}$/CCNF$_{4\%}$ hydrogels is 1.02 mS cm^{-1}, 0.98 mS cm^{-1}, 0.99 mS cm^{-1}, and 0.99 mS cm^{-1}, respectively, which is similar to the conductivity of the HDES$_{EG5}$ hydrogel. Excellent fracture strength is important, but the ability to withstand a wide range of strain (>400%) is also integral to flexible devices. To balance the excellent elongation and fracture strength, HDES$_{EG}$/CCNF$_{3\%}$ is chosen as the sample for the rest test. The hydrogel is connected in series with an orange LED bulb and tested by energizing it at a direct current voltage of 3 V. As illustrated in Fig. S9,† the orange LED bulb is successfully lit. Additionally, the brightness of the LED bulb decreases when the hydrogel is stretched to 2.5 times its initial length. When restored to the initial length of the hydrogel, the brightness of the LED bulb is also restored. This is mainly due to the increase of resistance caused by the decreased cross-sectional area and the increased length of the hydrogel with the increase of strain.

Moreover, the ability of energy dissipation of the HDES$_{EG}$/CCNF$_{3\%}$ hydrogel has been evaluated through the loading–unloading cycle test. The loading–unloading curves under different strains are illustrated in Fig. 3f. With the strain increased from 50% to 350%, the stress–strain curves show obvious hysteresis loops, suggesting that hydrogels can recover to the initial state through efficient energy dissipation.[43] And the increased dissipated energy and hysteresis are attributed to

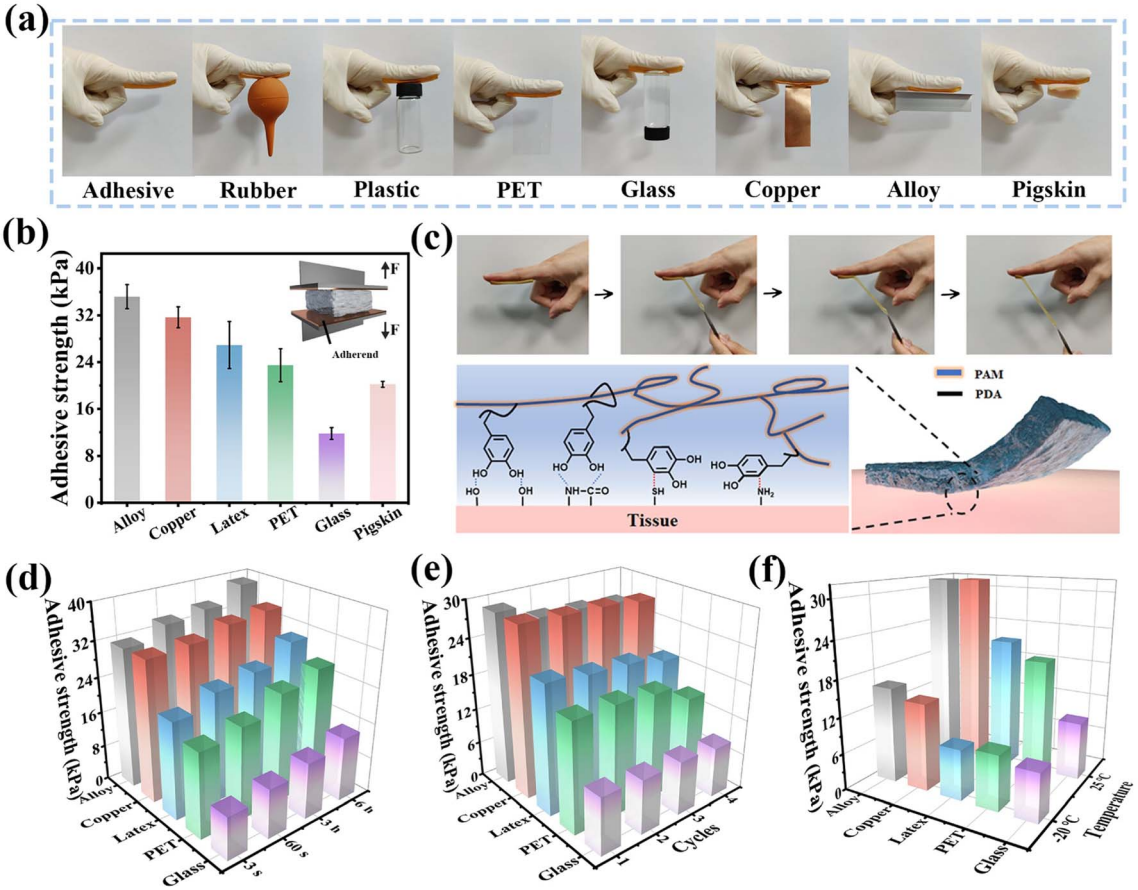

Fig. 4 (a) Photographs of the $HDES_{EG}/CCNF_{3\%}$ hydrogel adhered on various substrates. (b) The adhesive strength of the $HDES_{EG}/CCNF_{3\%}$ hydrogel to different substrates (1 min contact). (c) The process of peeling the hydrogel from the finger and diagram of the interaction between the tissue and hydrogel. (d) The adhesive strength of $HDES_{EG}/CCNF_{3\%}$ with different contact times. (e) The adhesive strength of $HDES_{EG}/CCNF_{3\%}$ with different cycles (3 s contact). (f) The adhesive strength of $HDES_{EG}/CCNF_{3\%}$ at different temperatures (3 s contact).

the destruction of sacrificial bonds and friction between CCNFs and polymers (Fig. S10a†). As shown in Fig. 3g, 10 cycles of hysteresis curves under 100% and 300% strains are tested without time intervals, and there is no obvious shifting and fracture, which means that the hydrogel possesses good fatigue resistance. The first loading–unloading of the two strains has a large hysteresis of about 25.90% (100%) and 28.62% (300%), and the dissipated energy of the hydrogel is 2.39 kJ m^{-3} and 18.48 kJ m^{-3} respectively (Fig. S10b and c†). Energy dissipation and hysteresis remain stable in the subsequent cycles, which is due to fracture and recombination of bonds reaching a relative balance and relaxation of polymer chains. Compressive strength is also an important index to evaluate the mechanical performance of hydrogels. To facilitate and accurately measure compression performance, the hydrogel surface is coated with flour and is subsequently dusted to remove excess powder for compression testing. The stress–strain curves of the $HDES_{EG}/CCNF_{3\%}$ hydrogel for compressive strength are evaluated in Fig. S11.† With the strain increasing, the stress enhanced rapidly, especially at 60–70%. The $HDES_{EG}/CCNF_{3\%}$ hydrogel is compressed for 10 cycles at 70% strain at a rate of 10 mm min^{-1} without time intervals, and it can be seen from the overlapping curves that the compressive strength of the hydrogel at 70% strain is almost completely recovered after stress removal (Fig. 3h). The curves illustrated the excellent recovery properties of the $HDES_{EG}/CCNF_{3\%}$ hydrogel.

3.3 Self-adhesive properties of $DES_{EG}/CCNF_{3\%}$

Hydrogels with self-adhesive properties can adapt to complex surfaces of various substrates in a manner that forms conformal contacts, which is especially helpful for the device to deliver clear and accurate signal feedback. In the presence of sufficient catechol groups, the hydrogels show no significant difference in load–displacement curves (Fig. S12a and b†). $HDES_{EG}/CCNF_{3\%}$ can adhere to various interfaces tightly, including rubber, plastic, polyethylene terephthalate (PET), glass, copper, alloy, and tissue (Fig. 4a). The catechol groups on PDA chains can form interactions with the adherend in the form of hydrogen bonds, electrostatic interactions, metal coordination, *etc.*[29,46] The adhesive strength in different interfaces is evaluated by a tensile-adhesion test, and pigskin is used to simulate human skin to be tested (Fig. S13†). As shown in Fig. 4b, the adhesive strength of the $HDES_{EG}/CCNF_{3\%}$ hydrogel on an alloy, copper, latex, PET, glass, and pigskin is 35.19, 31.66, 26.91, 23.47, 11.79,

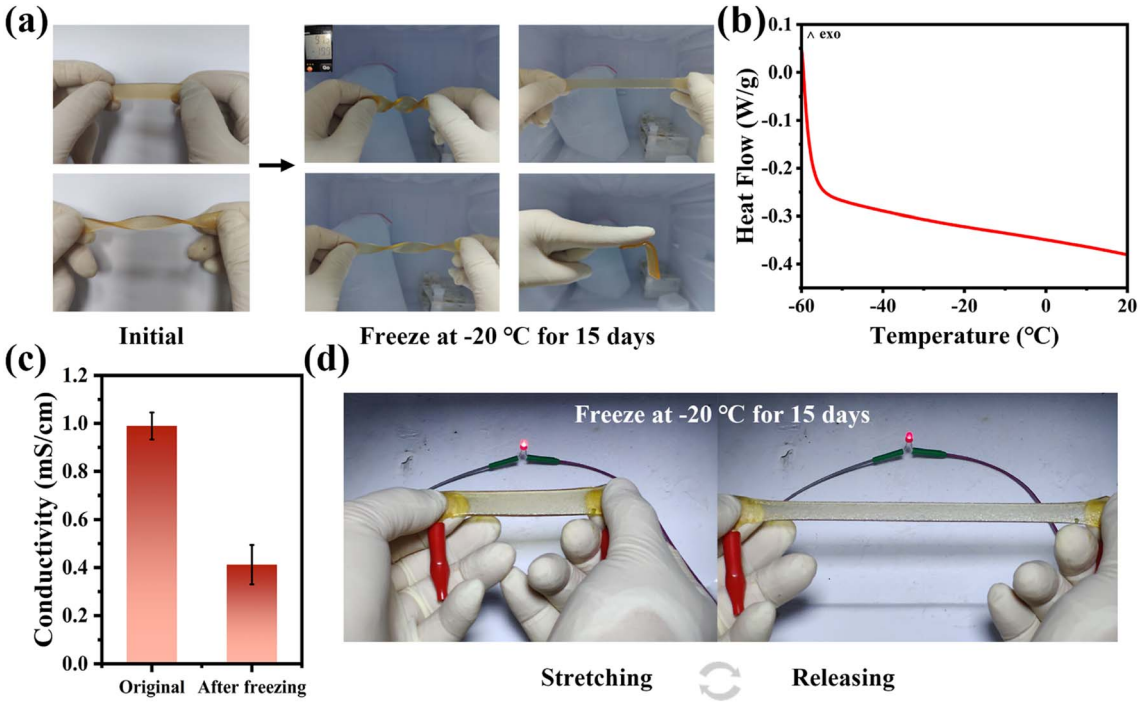

Fig. 5 (a) Photographs showing the flexibility and adhesion of the $HDES_{EG}/CCNF_{3\%}$ hydrogel in its initial state and after 15 days of freezing at −20 °C. (b) DSC curve of $HDES_{EG}/CCNF_{3\%}$ in the range of −60 to 20 °C. (c) The conductivity of the $HDES_{EG}/CCNF_{3\%}$ hydrogel in its initial state and after 15 days of freezing at −20 °C. (d) Photographs of brightness change of a LED lamp integrated with the $HDES_{EG}/CCNF_{3\%}$ hydrogel after 15 days of freezing at −20 °C during the stretching/release process.

and 20.20 kPa, respectively. The adhesion between hydrogels and plastics and glass is primarily influenced by hydrogen bonds and electrostatic interactions between catechol groups and the substrate interface. On the other hand, the adhesion between hydrogels and metals is primarily attributed to strong coordination effects. In Fig. 4c, it is shown that the $HDES_{EG}/CCNF_{3\%}$ hydrogel adheres to the finger of the volunteer stably and it takes a lot of force to peel the hydrogel from the skin. There are two kinds of interactions to assist to reach such a desirable adhesion effect. One is the transient and reversible non-covalent bonds, and the other is the strong and irreversible covalent bonds.[39] When the hydrogel is just in contact with tissue, the catechol groups can form hydrogen bonds with the surface groups of tissue, such as hydroxyl groups and peptide bonds. And initial adhesion is achieved with their help. After a period of time, the physiological environment of the tissue surface prompts the Michael addition reaction and the Schiff base reaction of the catechol group with –SH and $–NH_2$ respectively, which further enhance the adhesive strength of the $HDES_{EG}/CCNF_{3\%}$ hydrogel on the skin.

The adhesion properties of the hydrogel to substrates are further explored under different conditions. As the contact time increases, the adhesive strength of $DES_{EG}/CCNF_{3\%}$ shows an increasing trend, but the improvement is not significant, indicating that the interaction between the hydrogel and substrates is almost instantaneous (Fig. 4d). As the number of adhesions increases, the adhesion strength of the hydrogel shows a slight attenuation, implying the reliability of the hydrogel during multiple adhesion processes (Fig. 4e). As illustrated in Fig. 4f, the adhesion strength measured by freezing the hydrogel at −20 °C for 15 days (90% humidity) shows a significant decrease. The results are mainly attributed to the large amount of water adsorbed on the surface of the hydrogel, which blocks the contact of the catechol groups with substrates. The adhesive strength of the hydrogel shows slight differences in Fig. S12c,† which ensures reliable self-adhesive performance under different speed rates.

Furthermore, the $HDES_{EG}/CCNF_{3\%}$ hydrogel exhibits certain self-healing properties due to the hydrogen bonds and π–π stacking interactions among catechol groups. As illustrated in Fig. S14,† after the $HDES_{EG}/CCNF_{3\%}$ hydrogel is cut into two segments and re-contacted, the LED lamp in series with the $HDES_{EG}/CCNF_{3\%}$ hydrogel is re-lit under voltage drive and can remain lit when the hydrogel is stretched.

3.4 Anti-freezing and moisturizing properties of the $DES_{EG}/CCNF_{3\%}$ hydrogel

Hydrogels are a kind of material containing amounts of water, which inevitably freezes under sub-zero temperatures and forfeits the flexible and stretchable performance it was proud of. Due to the low melting point of DES_{EG}, the $HDES_{EG}/CCNF_{3\%}$ hydrogel exhibits excellent anti-freezing performance and the hydrogel is frozen at −20 °C for 15 days to characterize its freezing resistance. As shown in Fig. 5a, the $HDES_{EG}/CCNF_{3\%}$ hydrogel after freezing treatment still maintains excellent flexibility and can be stretched and twisted at random. It is worth

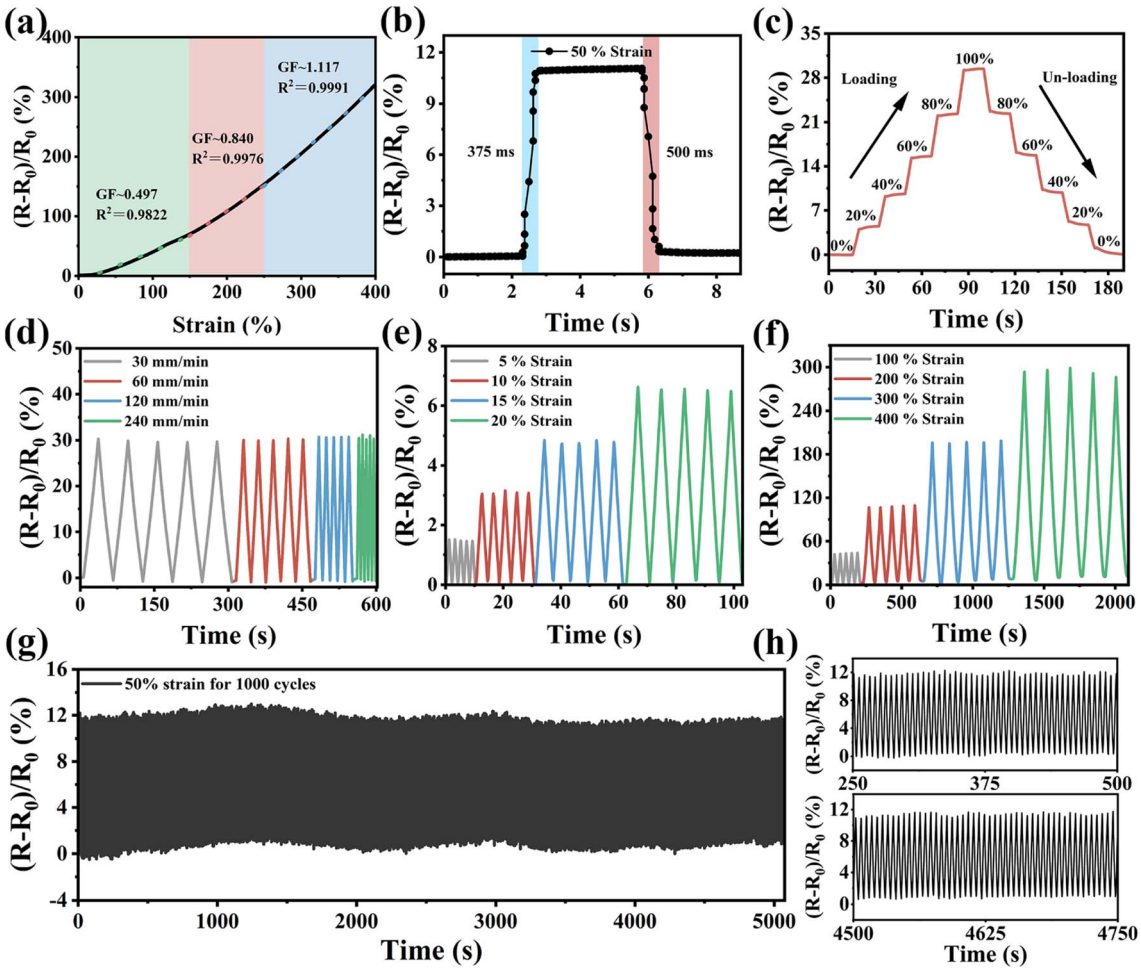

Fig. 6 (a) The sensitivity of the $HDES_{EG}/CCNF_{3\%}$ hydrogel in the strain range of 0–400%. (b) Response time of the $HDES_{EG}/CCNF_{3\%}$ hydrogel-based strain sensor at a strain of 50%. (c) A stepwise change in 20% strain from the strain range of 0–100–0%. (d) The strain of 100% at different stretching. (e) 5 stretching/releasing cycles in a small strain range, and (f) 5 stretching/releasing cycles in an enormous strain range. (g) 1000 cycle stability test of the $HDES_{EG}/CCNF_{3\%}$ hydrogel-based strain sensor at a strain of 50%. (h) Electrical signal at 250–500 s and 4500–4750 s in 1000 cycles, respectively.

noting that the $HDES_{EG}/CCNF_{3\%}$ hydrogel still possesses self-adhesive properties at low temperatures. As illustrated in Fig. 5b, the Differential Scanning Calorimetry (DSC) curve indicates that there is no glass transition in the range of −60 to 20 °C, which means that $HDES_{EG}/CCNF_{3\%}$ has anti-freezing properties. Moreover, the conductivity of the $HDES_{EG}/CCNF_{3\%}$ hydrogel has also been explored. As shown in Fig. 5c and S15,† $HDES_{EG}/CCNF_{3\%}$ possesses a conductivity of 0.41 mS cm^{-1} even after so many days of cryopreservation. The decreased conductivity can be attributed to the slower and restricted ion mobility.[47] The frozen treated hydrogel is connected in series with a LED bulb, and it is obvious that the bulb is lit up successfully, which proves that the $HDES_{EG}/CCNF_{3\%}$ hydrogel can work at sub-zero temperatures (Fig. 5d). And as the hydrogel stretched, the brightness decreased significantly, proving that the hydrogel still has good electrical responsiveness under harsh low-temperature conditions. The flexibility, self-adhesion, and conductivity of the $HDES_{EG}/CCNF_{3\%}$ hydrogel after freezing treatment all show that the hydrogel has the possibility of application under freezing conditions. The $HDES_{EG}/CCNF_{3\%}$ hydrogel shows excellent stretchability, admirable adhesive and anti-freezing properties, and the comprehensive performance is better than that in other research shown in Table S4.†

3.5 Sensing performance of $HDES_{EG}/CCNF_{3\%}$ hydrogel-based strain sensors

As obtained from the above study, $HDES_{EG}/CCNF_{3\%}$ shows excellent flexibility and shows a change in resistance with increasing strain, which has potential applications in resistive strain sensors. The sensing performance of the $HDES_{EG}/CCNF_{3\%}$ hydrogel-based strain sensor including sensitivity, response/recover time, and dynamic stability under different conditions is studied systematically in Fig. 6. As illustrated in Fig. 6a, the strain sensing curve can be divided into three linear regions: 0–150%, 150–250%, and 250–400%, and the corresponding linearities are 0.9822, 0.9976, and 0.9991, respectively. The gauge factor (GF) of the $HDES_{EG}/CCNF_{3\%}$ hydrogel

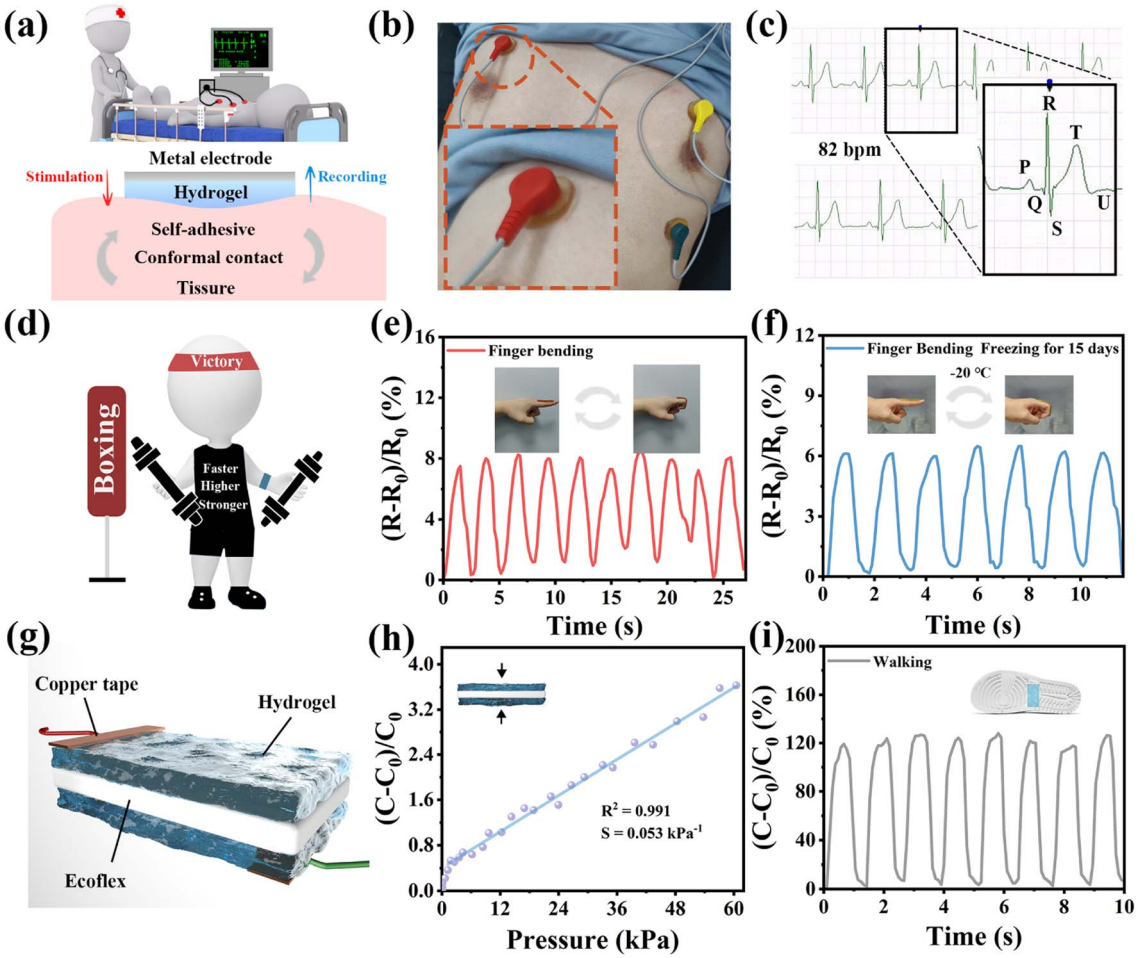

Fig. 7 (a) Diagram of application of the $HDES_{EG}/CCNF_{3\%}$ hydrogel to an ECG electrode patch for heartbeat detection. (b) A photograph of $HDES_{EG}/CCNF_{3\%}$ hydrogel electrodes attached to a volunteer. (c) Clear heart rate signals from a volunteer collected *via* $HDES_{EG}/CCNF_{3\%}$ hydrogel electrodes. (d) Diagram of application of the $HDES_{EG}/CCNF_{3\%}$ hydrogel-based strain sensor in motion monitoring. (e) and (f) Signal response of the $HDES_{EG}/CCNF_{3\%}$ hydrogel-based strain sensor during finger bending motion at room temperature and −20 °C. (g) Diagram of a $HDES_{EG}/CCNF_{3\%}$ hydrogel-based capacitive pressure sensor. (h) Relative capacitance changes of the $HDES_{EG}/CCNF_{3\%}$ hydrogel-based pressure sensor as a function of pressure. (i) Signal response of the $HDES_{EG}/CCNF_{3\%}$ hydrogel-based pressure sensor during walking.

corresponding to the three strain sensing ranges is 0.497, 0.840, and 1.117, respectively. Additionally, the strain sensor shows a fast response time of 375 ms under 50% strain and a recovery time of 500 ms to the initial state (Fig. 6b). The prompt response is helpful to convey signals to avoid misjudgment caused by unsynchronized movement and signal. As shown in Fig. 6c, a stepwise change in 20% strain from 0–100–0% strain demonstrates that relative resistance change in the stretching process corresponds to the release process, suggesting that the $HDES_{EG}/CCNF_{3\%}$ hydrogel-based strain sensor presents excellent stability and repeatability to face the complex situation.

Moreover, the cycle stability of the $HDES_{EG}/CCNF_{3\%}$ hydrogel-based strain sensor under different conditions is also tested, including rates and strains. The hydrogel sensor exhibits a stable electrical signal response for 5 consecutive stretching/releasing cycles at different tensile rates of 30, 60, 120, and 240 mm min^{-1} (Fig. 6d). Similarly, 5 cycles of consecutive stretching/releasing cycle tests are also performed on the hydrogel sensor under small (5%, 10%, 15%, and 20%) and large strains (100%, 200%, 300%, and 400%) respectively, and the relative resistance changes of the sensor signals under different strains are clear and stable with obvious distinctions (Fig. 6e and f). A long-term stability test of 1000 cycles is executed under 50% strain at 240 mm min^{-1} as shown in Fig. 6g. Comparing the relative resistance changes in two different periods, the $HDES_{EG}/CCNF_{3\%}$ hydrogel-based strain sensor possesses excellent cycling stability on the whole (Fig. 6h).

3.6 The application of the hydrogel flexible sensor and energy device

For clinical bioelectronic applications, poor interfacial contact between the skin and the electrodes can lead to a substantial decrease in stimulation and recording performance, whereas hydrogel-based epidermal electrodes with soft, conductive, self-adhesive properties have attracted extensive attention.[14] The

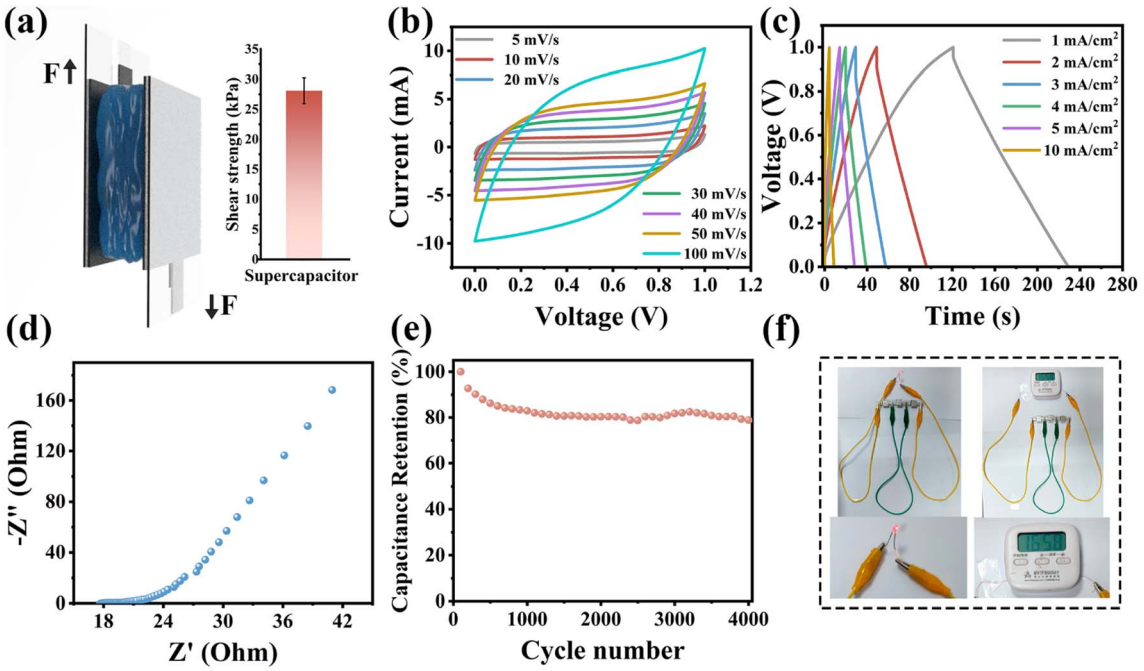

Fig. 8 (a) Diagram of the lap-shear method and shear strength between the hydrogel and electrodes. (b) CV curves at different scan rates. (c) GCD curves at different current densities. (d) EIS plot and (e) capacitance retention for 4000 cycles of the $HDES_{EG}/CCNF_{3\%}$ hydrogel-based supercapacitor. (f) Photographs of the $HDES_{EG}/CCNF_{3\%}$ hydrogel-based supercapacitor used to power the LED light and timer.

$HDES_{EG}/CCNF_{3\%}$ hydrogel with conductive, adhesive, and stretchable properties drives the possibility of application in bioelectrode patches and flexible sensors. The conformal contact between the interface of the hydrogel and the skin tissue ensures good contact, and the soft nature of the hydrogel ensures a mechanical match with the skin tissue (Fig. 7a). The $HDES_{EG}/CCNF_{3\%}$ electrode patch adheres between the metal electrode and the skin tissue of the volunteer to perform an ECG test (Fig. 7b). Due to the conformal contact generated at the interface, the ECG signal is clear and regular. The recorded heart rate of the volunteer is 82 beats per minute, and the six peaks commonly seen in ECG can be obviously distinguished in Fig. 7c. QRS wave groups can reflect the entire process of ventricular depolarization and can be used to understand the condition of the ventricular muscle and conduction system to help the physician make a diagnosis. In addition, the $HDES_{EG}/CCNF_{3\%}$ hydrogel is applied as a flexible sensor that adheres to the trunk of volunteers to conduct human motion detection (Fig. 7d). With the movement of tested parts (wrist, elbow, and knee), the relative resistance of the $HDES_{EG}/CCNF_{3\%}$ hydrogel-based strain sensor presents various degrees of alteration illustrated in Fig. S16.† The relative resistance change of wrist bending and knee bending is roughly 3 and 25 respectively, meaning that the regular and repetitive motion states can be monitored based on the waveform and its intensity and frequency. Moreover, finger bending at both room temperature and low temperature can be effectively detected by the sensor, and a stable relative resistance change can also be maintained after fifteen days of freezing at −20 °C, suggesting the reliability of applications in harsh environments (Fig. 7e and f). Besides the resistive stress–strain sensor, a simplified capacitive pressure sensor composed of Ecoflex as a dielectric layer, $DES_{EG}/CCNF_{3\%}$ hydrogels as electrodes, and 3M VHB tape as an encapsulation layer has also been prepared due to the excellent compression strength and reliable repeatability of the hydrogel (Fig. 7g). As shown in Fig. 7h, the relative capacitive change of the pressure sensor is detected between 0–60 kPa, which possesses a high linearity of about 0.991 and sensitivity (S) of 0.053 kPa^{-1} in the range of 3–60 kPa. The pressure sensor is used to monitor physical signal changes during human walking and the relative capacitance change is clear and steady as illustrated in Fig. 7i.

In addition, ionic conductive hydrogels are also widely used as solid-state electrolytes in supercapacitors. Fig. S17† shows the assembly diagram of a supercapacitor, and the active electrode is activated carbon (AC). A tighter interfacial contact is formed between the solid electrolyte and the electrodes without additional fixtures because of the robust adhesion of the $HDES_{EG}/CCNF_{3\%}$ hydrogel, which is beneficial to reduce the interface resistance and improve the performance of the supercapacitor. The strong adhesion is caused by the large number of hydrogen bonds formed between the groups on the surface of AC and catechol groups, such as –OH and –COOH. The adhesive strength is tested using the lap-shear method, which demonstrates excellent adhesion reliability up to 28.10 kPa (Fig. 8a). As shown in Fig. 8b, the cyclic voltammetry (CV) curves of this supercapacitor at different scan rates (5–100 mV s^{-1}) demonstrate the shape of quasi-rectangles, which is typical double-layer capacitive behavior. Under the current density from 1 to 10 mA cm^{-2}, the galvanostatic charge/discharge

(GCD) curves in Fig. 8c show almost symmetrical triangles. And the calculated specific capacitance is 108.37 mF cm^{-2} at a current density of 1 mA cm^{-2}. EIS shows that the intersection of the Nyquist curve and the *x* axis is the ohmic resistance produced by the electrolyte and the activated carbon electrode material, which is 17.87 Ω (Fig. 8d). The capacitance retention has also been tested at a current density of 5 mA cm^{-2} and is 78.88% after 4000 cycles, showing excellent stability (Fig. 8e). Three flexible supercapacitors connected in series can light up an LED bulb and power a timer as illustrated in Fig. 8f. The LED bulb is successfully lit up to emit red light and the timer works for 17 min, suggesting that $HDES_{EG}/CCNF_{3\%}$ shows great potential in supercapacitor applications as a solid electrolyte.

4. Conclusion

In summary, by adjusting the ratio of DES and the added CCNFs, we successfully synthesize an ionic-conductive hydrogel with excellent mechanical, self-adhesive, and anti-freezing/moisturizing properties. A 1 : 1 volume ratio of DES and alkali solution ensures the polymerization of DA and AM simultaneously. The catechol groups on PDA can form multiple interactions with substrates to achieve self-adhesive properties (20.20 kPa for skin). The intrinsic ionic conductivity of the DES endows the hydrogel with an excellent conductivity of 0.99 mS cm^{-1}. At the same time, the $HDES_{EG}/CCNF_{3\%}$ hydrogel has a weight ratio of 77.40% after being stored at room temperature for 7 days, and still maintains flexibility, adhesion, and conductive properties after being frozen at −20 °C for 15 days due to the low vapor pressure and low melting point of the DES. Moreover, the hydrogel exhibits excellent response time (375 ms) and cycling stability (1000 cycles), indicating its outstanding sensing performance. All these properties endow the $HDES_{EG}/CCNF_{3\%}$ hydrogel with a wide range of application scenarios. The hydrogel can be adhered to the skin as a bioelectrode for ECG recording and human motion monitoring and as a flexible sensor for wearable electronics applications (even at −20 °C), while a supercapacitor assembled with this hydrogel can light up an LED bulb and enable a timer to work for 17 minutes, showing great application potential.

Conflicts of interest

There are no conflicts to declare.

Acknowledgements

This work was supported by the National Science Foundation of China (NSFC, Grant No. 52373252), National High-Level Talents Special Support Program, Fundamental Research Funds for the Central Universities (2042023kf016, 2042022kf1052), Special Project on Knowledge Innovation of Wuhan (whkxjsj027), Fundamental Research, Key research and development project of Hubei Province (2022BCA040), and China Postdoctoral Science Foundation (2022TQ0239, 2022M722465).

References

1 K. Shen, Z. Liu, R. Xie, Y. Zhang, Y. Yang, X. Zhao, Y. Zhang, A. Yang and Y. Cheng, *Mater. Horiz.*, 2023, **10**, 2096–2108.
2 Z. Shen, Z. Zhang, N. Zhang, J. Li, P. Zhou, F. Hu, Y. Rong, B. Lu and G. Gu, *Adv. Mater.*, 2022, **34**, 2203650.
3 D. Wang, F. Yang, L. Cong, W. Feng, C. Wang, F. Chu, J. Nan and R. Chen, *Chem. Eng. J.*, 2022, **450**, 138025.
4 J. Liang, B. Tian, S. Li, C. Jiang and W. Wu, *Adv. Energy Mater.*, 2020, **10**, 2000022.
5 B. Tian, Y. Fang, J. Liang, K. Zheng, P. Guo, X. Zhang, Y. Wu, Q. Liu, Z. Huang, C. Cao and W. Wu, *Small*, 2022, **18**, 2107298.
6 X. Sun, F. Yao and J. Li, *J. Mater. Chem. A*, 2020, **8**, 18605–18623.
7 Q. Li, B. Tian, J. Liang and W. Wu, *Mater. Chem. Front.*, 2023, **7**, 2925–2957.
8 Y. Luo, M. Yu, Y. Zhang, Y. Wang, L. Long, H. Tan, N. Li, L. Xu and J. Xu, *Nano Energy*, 2022, **104**, 107955.
9 Y. Guo, L. Yang, L. Zhang, S. Chen, L. Sun, S. Gu and Z. You, *Adv. Funct. Mater.*, 2021, **31**, 2106281.
10 S. Wang, H. Cheng, B. Yao, H. He, L. Zhang, S. Yue, Z. Wang and J. Ouyang, *ACS Appl. Mater. Interfaces*, 2021, **13**, 20735–20745.
11 P. Guo, B. Tian, J. Liang, X. Yang, G. Tang, Q. Li, Q. Liu, K. Zheng, X. Chen and W. Wu, *Adv. Mater.*, 2023, **35**, 2304420.
12 O. Wichterle and L. Drahoslav, *Nature*, 1960, **185**, 117–118.
13 B. Ying and X. Liu, *iScience*, 2021, **24**, 103174.
14 H. Yuk, B. Lu and X. Zhao, *Chem. Soc. Rev.*, 2019, **48**, 1642–1667.
15 C. Jiang, T. Zhu, H. Liu, G. Yang, Z. He, M. Wang, M. Ji, G. Cong, J. Yu, C. Zhu and J. Xu, *J. Mater. Chem. A*, 2020, **8**, 22090–22099.
16 W. Ge, S. Cao, Y. Yang, O. J. Rojas and X. Wang, *Chem. Eng. J.*, 2021, **408**, 127306.
17 H. Zhang, N. Tang, X. Yu, Z. Guo, Z. Liu, X. Sun, M.-H. Li and J. Hu, *Chem. Eng. J.*, 2022, **430**, 132779.
18 X. Yao, S. Zhang, L. Qian, N. Wei, V. Nica, S. Coseri and F. Han, *Adv. Funct. Mater.*, 2022, **32**, 2204565.
19 T. Zhu, C. Jiang, M. Wang, C. Zhu, N. Zhao and J. Xu, *Adv. Funct. Mater.*, 2021, **31**, 2102433.
20 Q. Zhang, K. De Oliveira Vigier, S. Royer and F. Jerome, *Chem. Soc. Rev.*, 2012, **41**, 7108–7146.
21 Z. Luo, W. Li, J. Yan and J. Sun, *Adv. Funct. Mater.*, 2022, **32**, 2203988.
22 J. D. Mota-Morales and E. Morales-Narváez, *Matter*, 2021, **4**, 2141–2162.
23 L. Han, K. Liu, M. Wang, K. Wang, L. Fang, H. Chen, J. Zhou and X. Lu, *Adv. Funct. Mater.*, 2018, **28**, 1704195.
24 S. Wang, Y. Fang, H. He, L. Zhang, C. A. Li and J. Ouyang, *Adv. Funct. Mater.*, 2020, **31**, 2007495.
25 W. Zhang, R. Wang, Z. Sun, X. Zhu, Q. Zhao, T. Zhang, A. Cholewinski, F. K. Yang, B. Zhao, R. Pinnaratip, P. K. Forooshani and B. P. Lee, *Chem. Soc. Rev.*, 2020, **49**, 433–464.

26 B. Xue, J. Gu, L. Li, W. Yu, S. Yin, M. Qin, Q. Jiang, W. Wang and Y. Cao, *Nat. Commun.*, 2021, **12**, 7156.
27 S. Hu, X. Pei, L. Duan, Z. Zhu, Y. Liu, J. Chen, T. Chen, P. Ji, Q. Wan and J. Wang, *Nat. Commun.*, 2021, **12**, 1689.
28 J. H. Ryu, P. B. Messersmith and H. Lee, *ACS Appl. Mater. Interfaces*, 2018, **10**, 7523–7540.
29 C. Zhang, B. Wu, Y. Zhou, F. Zhou, W. Liu and Z. Wang, *Chem. Soc. Rev.*, 2020, **49**, 3605–3637.
30 C. Xie, X. Wang, H. He, Y. Ding and X. Lu, *Adv. Funct. Mater.*, 2020, **30**, 1909954.
31 S. Hong, Y. Yuan, C. Liu, W. Chen, L. Chen, H. Lian and H. Liimatainen, *J. Mater. Chem. C*, 2020, **8**, 550–560.
32 G. Ge, K. Mandal, R. Haghniaz, M. Li, X. Xiao, L. Carlson, V. Jucaud, M. R. Dokmeci, G. W. Ho and A. Khademhosseini, *Adv. Funct. Mater.*, 2023, **33**, 2207388.
33 C. D'Agostino, L. F. Gladden, M. D. Mantle, A. P. Abbott, E. I. Ahmed, A. Y. M. Al-Murshedi and R. C. Harris, *Phys. Chem. Chem. Phys.*, 2015, **17**, 15297–15304.
34 O. S. Hammond, D. T. Bowron and K. J. Edler, *Angew Chem. Int. Ed. Engl.*, 2017, **56**, 9782–9785.
35 S. Rozas, C. Benito, R. Alcalde, M. Atilhan and S. Aparicio, *J. Mol. Liq.*, 2021, **344**, 117717.
36 B. B. Hansen, S. Spittle, B. Chen, D. Poe, Y. Zhang, J. M. Klein, A. Horton, L. Adhikari, T. Zelovich, B. W. Doherty, B. Gurkan, E. J. Maginn, A. Ragauskas, M. Dadmun, T. A. Zawodzinski, G. A. Baker, M. E. Tuckerman, R. F. Savinell and J. R. Sangoro, *Chem. Rev.*, 2021, **121**, 1232–1285.
37 K. Haraguchi and T. Takehisa, *Adv. Mater.*, 2002, **14**, 1120–1124.
38 X. Yang, S. K. Biswas, J. Han, S. Tanpichai, M. C. Li, C. Chen, S. Zhu, A. K. Das and H. Yano, *Adv. Mater.*, 2021, **33**, 2002264.
39 H. Jung, M. K. Kim, J. Y. Lee, S. W. Choi and J. Kim, *Adv. Funct. Mater.*, 2020, **30**, 2004407.
40 L. Han, L. Yan, K. Wang, L. Fang, H. Zhang, Y. Tang, Y. Ding, L.-T. Weng, J. Xu, J. Weng, Y. Liu, F. Ren and X. Lu, *NPG Asia Mater.*, 2017, **9**, e372.
41 H. Montazerian, A. Baidya, R. Haghniaz, E. Davoodi, S. Ahadian, N. Annabi, A. Khademhosseini and P. S. Weiss, *ACS Appl. Mater. Interfaces*, 2021, **13**, 40290–40301.
42 S. Choi, Y. j. Choi, M. S. Jang, J. H. Lee, J. H. Jeong and J. Kim, *Adv. Funct. Mater.*, 2017, **27**, 1703826.
43 Y. Wei, L. Xiang, H. Ou, F. Li, Y. Zhang, Y. Qian, L. Hao, J. Diao, M. Zhang, P. Zhu, Y. Liu, Y. Kuang and G. Chen, *Adv. Funct. Mater.*, 2020, **30**, 2005135.
44 X. Nie, L. Miao, W. Yuan, G. Ma, S. Di, Y. Wang, S. Shen and N. Zhang, *Adv. Funct. Mater.*, 2022, **32**, 2203905.
45 H. Huang, J. Yun, H. Feng, T. Tian, J. Xu, D. Li, X. Xia, Z. Yang and W. Zhang, *Energy Storage Mater.*, 2023, **55**, 857–866.
46 S. Li, H. Zhou, Y. Li, X. Jin, H. Liu, J. Lai, Y. Wu, W. Chen and A. Ma, *J. Colloid Interface Sci.*, 2022, **607**, 431–439.
47 Y. Ye, Y. Zhang, Y. Chen, X. Han and F. Jiang, *Adv. Funct. Mater.*, 2020, **30**, 2003430.